Optimal fingerprinting of the upper 2000m of the ocean for forecasting heat content trends

A Thesis Presented
By
Henry Dowling
to

The department of Applied Mathematics
in partial fulfillment of the requirements
for a degree of Bachelor of Arts

March 2022
Harvard College

Optimal fingerprinting of the upper 2000m of the ocean for forecasting heat content trends

Abstract

Anthropogenically-induced ocean heat uptake is an important climate variable, whose future value has implications in the expected pattern of sea-level rise, climate sensitivity, and extreme weather events. However, trends in ocean heat content (OHC) due to forcing are difficult to detect. As a result of its large thermal mass, the three-dimensional ocean heats slowly, whereas the near-surface ocean experiences great variations in temperature on annual and interannual timescales. Fingerprinting is a useful technique for identifying a weak signal amidst noisy data. It has been used successfully for detection of anthropogenic influence in a variety of climate variables, such as near-surface air temperature, sea surface temperature, and sea ice extent. OHC is therefore a promising potential application for this technique, yet horizontally-sliced fingerprinting on three-dimensional OHC has not been attempted. An optimal fingerprint analysis is applied on 100 years of synthetic historical OHC data from the ACCESS-ESM1-5 climate model from the time period 1850-1900 and 15 years of Argo data 2004-2018, on 15 5-degree-gridded constant-pressure level surfaces in the upper 2000m. We propose a modified fingerprinting approach in which the primary modes of thermal variability— those caused by the annual cycle and ENSO—are controlled for before the fingerprint is computed.We derive an optimal fingerprint for detecting change in OHC in 34 pressure levels in the upper 2000m of the ocean. We find that the optimal fingerprint for OHC has strongly positive coefficients in the western Pacific; this can likely be ascribed to the the relative quiescence of this region. Despite a generally positive trend, the optimal fingerprint is characterized by negative coefficients in the upper North Atlantic. The optimal fingerprint resembles the anticipated signal direction increasingly with depth, highlighting the value of examining three-dimensional OHC. We compute optimal detection variables corresponding to these fingerprints, and determine that the upper 2000m has seen instances significant increase in heat content over the last 15 years.

Contents

Acknowledgments

I AM DEEPLY grateful to several people, without whom this work would not exist. First and foremost, I would like to thank Peter Huybers for his unwavering support and constant flow of endlessly helpful suggestions, questions, and ideas. He was infinitely generous with his time and greeted my incessant pestering with nothing but warmth, despite his busy research schedule.

I would also like to extend my gratitude to Carl Wunsch for helping to advise this thesis, and for his very helpful feedback on my first draft. I knew next to nothing about oceanography before embarking on this project, and Carl's guidance was immensely helpful in getting me up to speed.

Thanks as well to the rest of the Huybers group– especially Duo Chan and Charlotte Dyvik Henke– for their support and assistance, and for many helpful discussions which greatly informed my research.

There are several students I would like to thank: Candice Chen, for very kindly helping me to learn climate science as a complete beginner, and for providing helpful suggestions when I found myself blocked in my research. Alex Chin, for nonstop advice about how to do research, tips on handling large matrices on a small computer, and unconditional emotional support. And Rajath Salegame, for entertaining my frequent questions about Python and data science in general.

Thanks as well to the Applied Math department, and especially Margo Levine, for helping me to organize my thoughts around my decision to write a thesis, and for helping me in the process of choosing an advisor.

Finally, I would like to express my deepest thanks and gratitude to my parents and my entire family, for supporting me without hesitation in my academic endeavours.

Listing of figures

1

Introduction

1.1 Ocean heat content

The oceans are the dominant component of climatic thermal inertia on Earth. (Resplandy et al., 2019). Not only do the oceans make up about 70% of the surface of the Earth, but also the physical properties of oceans allow for greater heat absorption than land. Water has a higher specific heat than the most of the land surface of Earth. In addition, because water is a

fluid, heat thus transported to depth much much more effectively in the oceans than on land via convection– the ocean's wind-driven mixed layer can extend to several hundred meters in certain regions (de Boyer Montégut et al., 2004). Heat is transported to even greater depths by physical processes such as general circulation, albeit on much longer timescales, which can exceed 1000 years in certain regions (Gebbie & Huybers, 2019). As a result of these physical properties, although oceans comprise just 70% of the surface of the planet, they have taken up around 90% of the excess heat generated by anthropologically-induced warming (Church et al., 2011).

1.2 Why care about ocean heat content?

An understanding of the evolution of ocean heat content is essential to forecasting the planet's response to climate change. Because a large proportion of the thermal energy of the climate system is stored in the ocean, a first-order implication of a better characterization of heat content in the ocean is an improved understanding of the way the climate as a whole responds thermally to changes in forcing. For example, estimations of equilibrium and transient climate sensitivity could be significantly improved with a better understanding of the behavior of OHC (Lyu et al., 2021). Ocean heat also has a meaningful influence on the patterns of ice melt and formation, hence better knowledge of how OHC changes over time would allow better models of such phenomena (Smith et al., 2018).

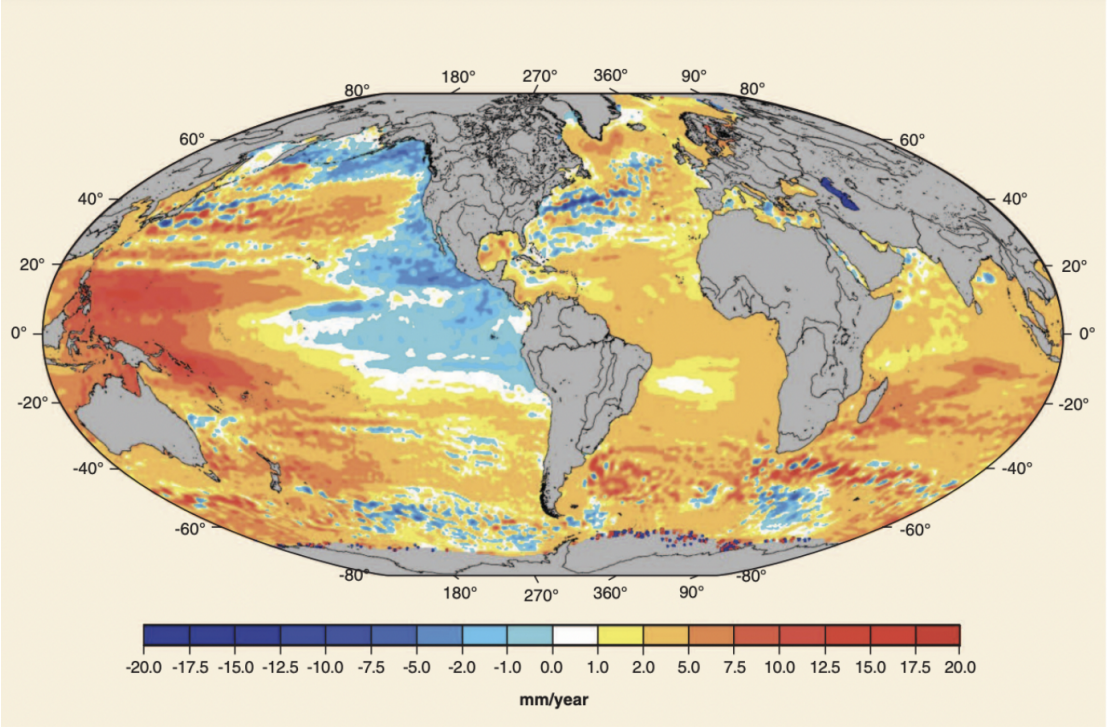

Figure 1.1: Annual rate of sea level rise over the period October 1992 to July 2009, as determined by satellite altimetry from Topex/Poseidon, Jason-1 & -2, GFO, ERS-1 & -2, and Envisat. (Nicholls and Cazenave, 2010).

1.2.1 Sea levels

Changes in ocean heat content are closely linked to the pattern of sea level rise. H_2O expands in response to changes in temperature above 4°, with a thermal expansion coefficient of roughly 2.1e-4 *. Therefore, changes in heat content to a column of water–equally at depth and near the surface–raise the level of the column of water. This phenomenon represents an important vertical teleconnection between the deep ocean and the surface. The heating of

*It is worth noting that oceanic thermal expansion is also a function of pressure and salinity, so heat effects are not necessarily linear.

the oceans due to anthropogenic forcing contributes significantly to sea level rise: the global mean thermosteric component of sea level rise has been measured at 0.5mm/yr for 1955-2010, accounting for around 30% of sea level rise over that time period (Levitus et al., 2012). Regional anomalies in ocean heat content, salinity, and ice melt cause spatial non-uniformity in sea-level rise. Current annual sea-level trends vary from roughly -5mm/year to +10mm/year (see figure 1.1)

Although it is well-established that the global mean sea level will rise over the next century as a consequence of climate change, there is large uncertainty about the rate of this rise, as well as its spatial pattern (Church et al., 2013). A better understanding of the future evolution of ocean heat content will permit greater confidence in estimates of these quantities. Given that an estimated 1 billion people live below 10m elevation, with 230 million of those living below 1m elevation, this could have important consequences to the global strategy of adaptation to climate change (Kulp & Strauss, 2019).

1.2.2 Other effects of changing heat content

Ocean warming has also been shown to alter marine habitats considerably Jorda et al. (2020). The pattern and magnitude of ocean heat content trends due to climate change therefore carry immediate consequences in conservation. The strength of interannual climatic oscillations such as El-Niño are also believed to be affected by ocean heat content.

1.3 Measuring changes in Ocean Heat Content

Measuring the subsurface ocean is difficult. Unlike the atmosphere, light does not penetrate more than a few meters in the ocean, making observation by indirect means difficult. Although regular measurement of sea surface temperatures dates back centuries, the only source of data on subsurface ocean temperatures up until the 21st was ship-based measurements, which are sparse and ultimately inadequate to construct an accurate picture of the deep ocean (Wunsch, 2015). Scientific understanding of the deep ocean was revolutionized in 2004 by the launch of the Argo profiling float program, an international project that deploys thousands of floats that automatically measure various physical properties of interest in the ocean, such as temperature, salinity, and pressure, and surface at regular intervals to report their measurements via satellite. Unlike ship-based measurements, Argo floats provide a high density of reliable data at depths up to 2000m.

1.3.1 Natural thermal variability in the ocean

Thanks to Argo floats, a picture of the thermal structure of the upper 2000m of the ocean has emerged. The data have revealed complex spatial non-uniformities and high variabilities even below the region of rapid temperature change known as the thermocline (figure 1.2). The dynamics of thermal variability of the upper 2000m of the ocean is not entirely understood. It stems from the combination of a number of interrelated processes, including cycles

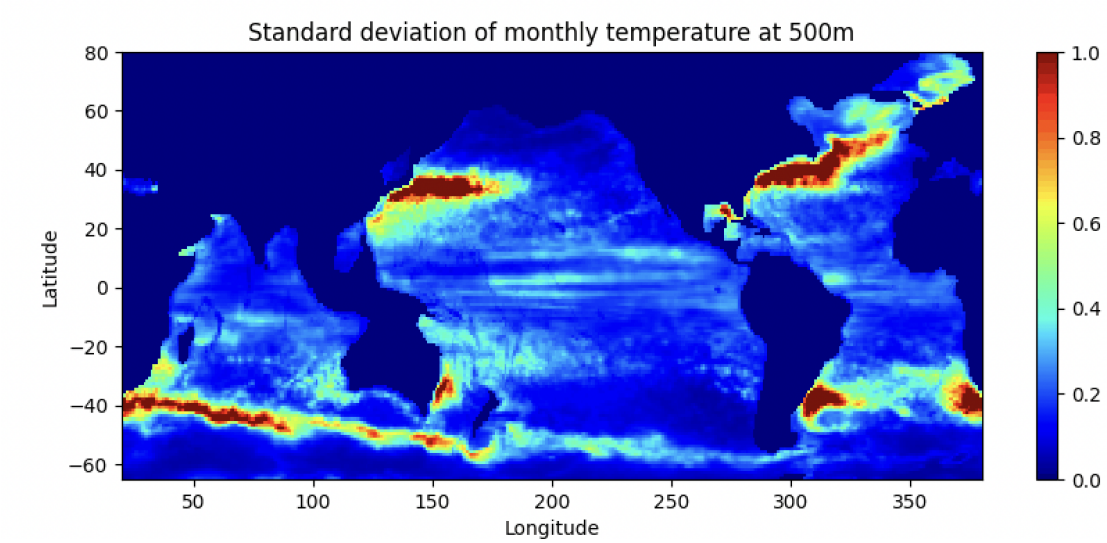

Figure 1.2: Temporal standard deviation (°C) of annual mean temperature at 500m over the period 2004-2018. Data is from Argo floats. Note the well-resolved spatial patterns: currents due to gyre circulation in the North Atlantic and Northwest Pacific are clearly visible, as well as the circumpolar current.

of annual and interannual variability such as El Niño-Southern Oscillation (ENSO) and the Northern Atlantic Oscillation, circulation patterns, ocean weather, and interaction with the atmosphere (Penduff, 2018). The ocean varies appreciably on multi-decadal timescales (examples of this are the Interdecadal Pacific Oscillation and the Atlantic Multi-decadal Oscillation), making it difficult to determine average values of any ocean statistic since reliable data have only been available for about 15 years (Wunsch, 2020). Ocean heat content in the upper 2000m represents an intricate and richly non-uniform system, both spatially and temporally.

1.4 Optimal Fingerprinting

Optimal fingerprinting is a mathematical tool that is useful for determining the strength of a weak signal of a known pattern in a noisy dataset. Because of the high thermal variability of the upper ocean, and the slow rate at which the ocean warms due to external forcing, this thesis applies this technique to horizontally-mapped three-dimensional ocean heat content. Here, we will briefly past applications of fingerprinting to analyze weak climate variables in large noise fields.

Optimal fingerprinting was first introduced to the field of climate science in a 1979 paper by physical oceanographer Klaus Hasselmann[†], who proposed the application of a standard technique from signal processing theory to the problem of determining which climate variables are best suited to detecting anthropogenic climate change (Hasselmann, 1979). Hasselmann introduced the term "optimal fingerprinting" to this technique in a 1993 follow-up paper (Hasselmann, 1993). An optimal fingerprint of a signal, as by Hasselmann's description, is a vector in climate variable-space (i.e. the space of the possible observations that could be made of multiple climate variables, such as sea-surface temperature or atmospheric air pressure) which points in the direction optimal for detection of the signal. Hasselmann observed that this direction might not be parallel to that of the signal– for instance, in the case that some climate variables are noisier than others (and thus should be weighted less heavily to

[†]A recent Nobel laureate!

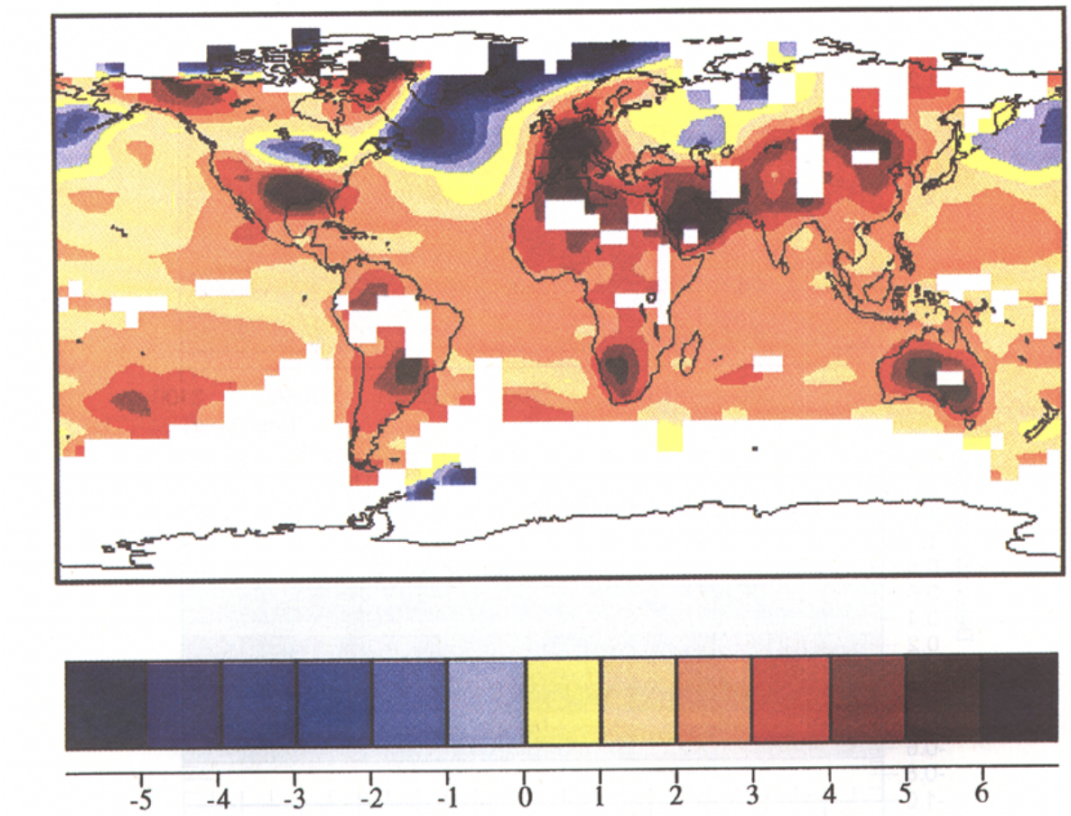

Figure 1.3: The optimal fingerprint derived by Hegerl et al. (Hegerl et al., 1996)

increase the signal-to-noise ratio). Hegerl et al. applied this technique to near-surface air-temperature trends, computing an optimal fingerprint and using their findings to determine claim that the probability that observed climate conditions were a result of natural variability rather than anthropogenic influence was less than 5% (Hegerl et al., 1996).

Fingerprinting has previously been used successfully in applications on ocean heat content. Barnett et al. examined vertical patterns of ocean heat content change, and found statistically significant human-induced warming (Barnett et al., 2004). Similarly, Glecker et al. examined

a large pool of observational and model-generated data to calculate optimal fingerprints for basin-average upper-ocean temperature changes, also finding positive evidence of an anthropogenic impact (Glecker et al., 2012).

Optimal fingerprinting has also been applied effectively to a number climate variables other than ocean heat content. Hobbs et al. uses fingerprinting to examine whether recent sea-ice extent data can be adequately explained by internal variability (Glecker et al., 2015). Min et al. employ fingerprinting in a study of extreme precipitation events, finding that in the majority of Northern Hemisphere land for which sufficient data is available, human influence has contributed appreciably to such events (Min et al., 2011).

2

Optimal Fingerprinting

2.1 Motivation

Optimal fingerprinting is a standard method for identifying a signal in a noisy dataset. We will briefly provide a motivation for optimal fingerprinting here. Suppose we have a dataset P of n-dimensional data $P \subset \mathbb{R}^n$ consisting of a set of observations $p_i \in P$. Suppose further that we wish to determine the magnitude of a signal $\psi_s = cg$ in the dataset whose direction

$g \in R^n$ is known, but whose magnitude $c \in \mathbb{R}$ is not. For example, g may be determined from an understanding of climate dynamics or through climate modeling. A simple approach for computing this value from observational data is to project the observations onto the signal, yielding a "detection variable" d_s whose magnitude corresponds to the strength of the signal in the observations:

$$d_s = \langle \pi(s, p_i) \rangle \tag{2.1}$$

where $\langle\rangle$ indicates the mean over the set of observations p_i in P. This is a reasonable approach, however, it offers limited utility when the dataset P is noisy in the direction of the anticipated signal, as in this case the detection variable will itself be very noisy. In order to rectify this, it is desirable to weight the detection variable towards low-noise dimensions of P.

2.2 Definition

Fingerprinting provides a rigorous way to conduct this weighting. We wish to find a vector $f \in \mathbb{R}$ which, when our set of observations P is projected onto it, yields a detection variable d_f which maximizes the squared signal-to-noise ratio for our signal s. Formally, we wish to find f such that the quantity R^2 as defined below is maximized:

$$R^2 = \frac{(d_{f,\psi})^2}{\langle d_{f,p_i} \rangle} \tag{2.2}$$

where

$$d_{f,\psi} = f^T \psi_s \tag{2.3}$$

and

$$d_{f,p_i} = f^T p_i. \tag{2.4}$$

Solving (2.2) yields

$$f = C^{-1} g \tag{2.5}$$

where $C \in \mathbb{M}_{n \times n}$ is the covariance matrix of the dataset P over its n dimensions Hasselmann (1993). The optimal detection variable d_f^* is then given by

$$d_f^* = \langle f^T p_i \rangle \tag{2.6}$$

The determination C can be made from observational or model data, although it is rather difficult in practice for high-dimensional data sets as an insufficient quantity of observational can lead to this matrix being significantly underdetermined Hegerl et al. (1996).

2.3 An example: detecting climate change in atmospheric temperature

One of the first uses of fingerprinting in climate science was towards the detection of anthropogenic climate change in atmospheric temperatures. Here we briefly show how finger-

printing can be used in application to demonstrate the usefulness of maximizing the signal-to-noise ratio.

Suppose that from model runs, is has been determined that anthropogenic climate change is characterized by a warming of the troposphere and a cooling of the stratosphere, and the ratio of their warming and cooling is expected to satisfy

$$x = cy \tag{2.7}$$

where x is the rate of stratospheric warming in $^\circ$ C/yr (we expect that the component of x due to climate change will be negative here), and y is the rate of tropospheric warming in $^\circ$C/yr. We can then think of the "direction" of the signal $s \in \mathbb{R}^2$ of climate change as $[-1, c]$.

Now, suppose that through climate modeling, we are able to understand the structure of the natural patterns of temperature variation in the troposphere and stratosphere. Suppose for our example that they're both normally distributed with a mean of 0 and variances of σ_s^2 and σ_t^2 for the stratosphere and thermosphere respectively, and that they covary by q. Then, we can write the covariance matrix of natural variability C as

$$C = \begin{bmatrix} \sigma_t^2 & q \\ q & \sigma_s^2 \end{bmatrix} \tag{2.8}$$

Then, by (2.5), the optimal fingeprint for this detection problem f is given by

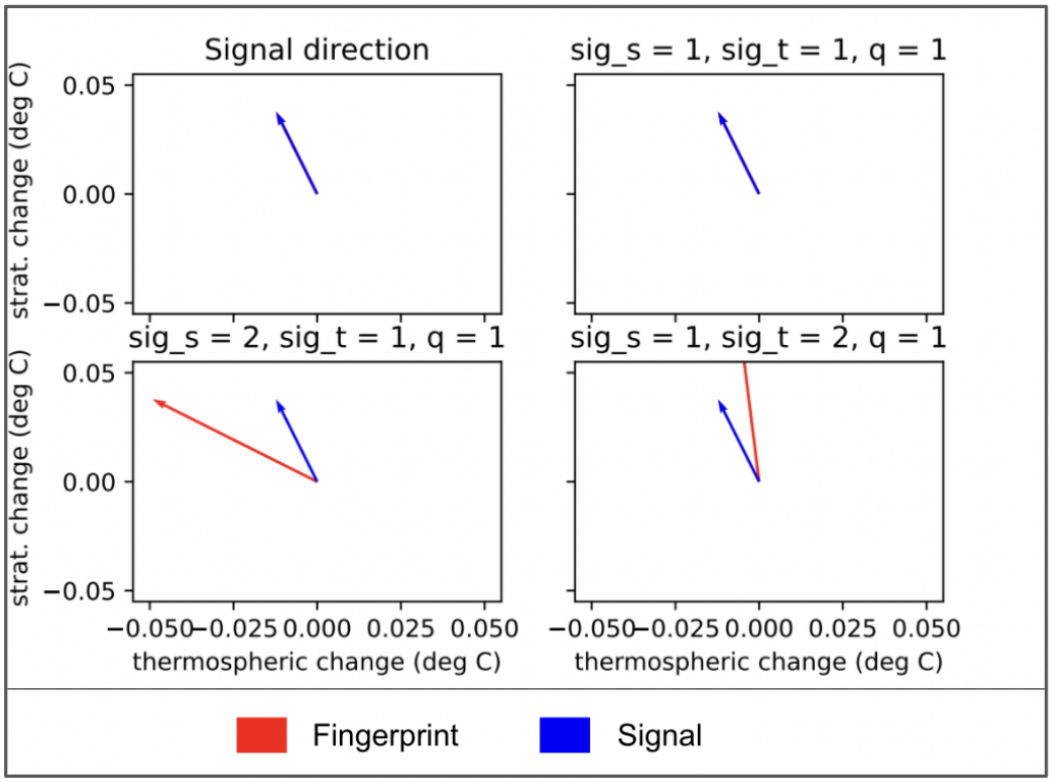

Figure 2.1: Optimal fingerprint direction for the atmospheric warming example with different noise levels in each climate variable.

$$f = \begin{bmatrix} \sigma_t^2 & q \\ q & \sigma_s^2 \end{bmatrix} \begin{bmatrix} 1 \\ -c \end{bmatrix} \tag{2.9}$$

$$= \begin{bmatrix} \sigma_t^2 - qc \\ q - \sigma_s^2 \end{bmatrix}. \tag{2.10}$$

Figure (2.2) gives the direction of the optimal fingerprint for several values of σ_t, σ_s, and q.

Observe that in the upper left panel, where each climate variable has an equal variance, the optimal fingerprint direction coincides with that of the signal, even if the variables have some covariance. In the bottom left and bottom right panels, observe that fingerprint is weighted towards the direction of the variable which has a lower value of σ, indicating lower noise. Hence, an optimal fingerprint can be understood intuitively as (and is equivalent in the case $n = 2$ to) a vector in climate-space whose value is equal to the coefficients of the signal divided by their "noisiness".

3

Application of fingerprinting to ocean heat content

We now apply the technique of optimal fingerprinting to measurements of ocean heat content, examining 15 pressure levels in the upper 2000m. Ocean heat content proves to be resistant to a naive application of optimal fingerprinting, due to its strong modes of interan-

nual variability. We thus adapt the fingerprinting method to the ocean by first accounting for the major modes of oceanic thermal variability, computing fingerprints against natural variability covariance matrices with these modes subtracted. We make use of standard statistical techniques to recover an approximate inverse of the covariance matrix of natural variability when it is noninvertible.

3.1 Methods

We use data generated by the ACCESS-ESM 1-5 climate model to estimate the covariance of natural ocean variability and determine the anticipated signal of ocean heat content change from a multiple linear regression on Argo data, estimating the inverse covariance matrix with linear algebraic techniques. We further refine our fingerprint by accounting for strong modes of natural variability in model data, and provide estimations of the optimal climate detection variable at depth levels ranging from 0-2000m.

3.1.1 Data

Observational data used to compute the optimal fingerprint is obtained from the Roemmich-Gilson Argo monthly temperature and salinity climatology, years 2004-2018. Years 2018-2021 are omitted to ensure the principal modes of thermal variability are accurately determined for all years in our observational period (see section 4). Potential temperature at depths 0-2000m is calculated from Argo temperature, salinity, and pressure means and anomalies.

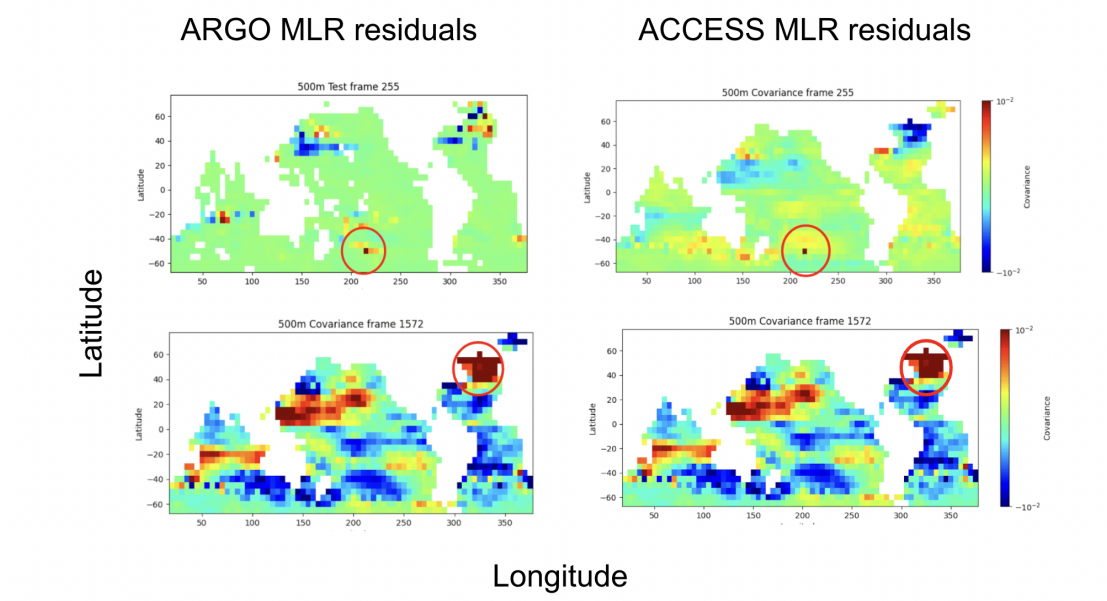

Figure 3.1: Covariances of two representative points in residuals from multiple-linear-regressions performed on Argo observational data and ACCESS model data. Their similarity indicates the skill of the ACCESS-ESM-1.5 model for our use case.

Potential temperature data is then averaged to 4.5 × 5 degree longitudinal/latitudinal resolution and annualized. This resolution was chosen due to computational constraints. Latitudes above 65 ° N and below 65 ° S are omitted. Data is regridded longitudinally and vertically to align with model data.

Model data used in the computation of an optimal fingerprint is obtained from historical forced simulations 1850-2020 from the ACCESS-ESM1-5 model (Australian Community Climate and Earth System Simulator), a member of CMIP6 (Ziehn et al., 2019) The ACCESS model was chosen due to its large number of model runs, which is a necessary for a sufficiently determined error covariance matrix of natural variability. The ocean dynamics in the ACCESS model are sourced from the GFDL MOM5 ocean model. Only data from 1850-1900 is considered, as the purpose of the model data for our application is to simulate unforced natural variability. Early historical forced data is used rather than unforced simulations (of which some are available from ACCESS) because more model runs are readily available of the forced simulation. As with Argo data, temperature data is averaged to 4.5 × 5 degree longitudinal/latitudinal resolution and annualized. Latitudes above 65 ° N and below 65 ° S are omitted.

3.1.2 Modes of ocean thermal variability

In order to generate a useful covariance matrix of ocean temperatures for our fingerprint, the most powerful modes of ocean thermal variability must be accounted for. The primary

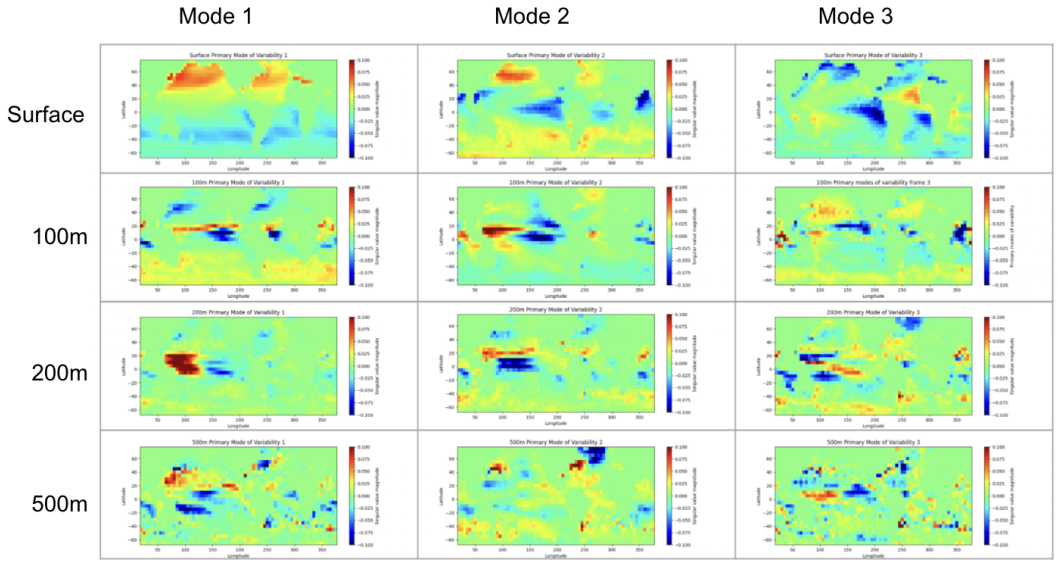

Figure 3.2: Three largest modes of variability, as determined by singular value decomposition, on monthly Argo data (n = 180) gridded at 4.5x5 degrees lat x long. The annual cycle clearly accounts for the strongest mode in the near-surface ocean, but its influence is significantly weaker below the mixed layer. ENSO accounts for the remaining modes in the near-surface ocean. At 500m, the influence of ENSO is also less prominent, although it is still visible.

modes of ocean thermal variability were determined via singular value decomposition of monthly Argo temperature timeseries data at each pressure level. The primary modes of variability are depicted in figures 3.2 and 3.3. The main patterns of thermal variability appear to agree with the annual cycle and ENSO. Hence, in order to control for these modes when performing our fingerprint, we first annualize the data and then regress ocean heat content against ENSO3.4, which is a typical proxy for the strength of ENSO in a given month, the Hilbert transform of ENSO3.4, and linear time. We model the potential temperature θ of a given location as a function of time as

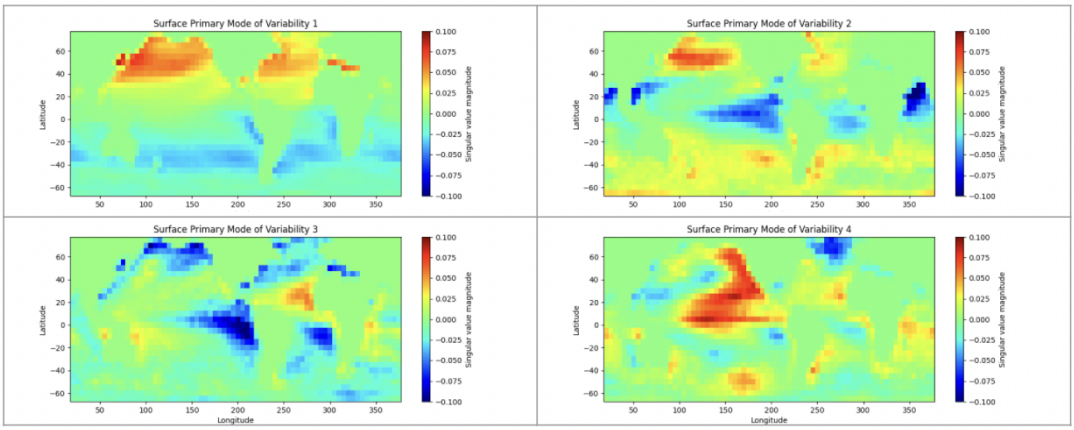

Figure 3.3: The four largest modes of annual variability at the ocean's surface, determined by singular value decomposition, on monthly Argo data (n = 180) gridded at 4.5x5 degrees lat x long.

$$\theta(t) = (a_1 \times t) + (a_2 \times E) + (a_3 \times H) + e(t) \tag{3.1}$$

where E is the cf the ENSO3.4 index, H is the value of the Hilbert transform of the ENSO3.4 index, a_1 corresponds to the time coefficient of regression, a_2 corresponds to the ENSO3.4 coefficient of regression, and a_3 corresponds to the Hilbert-transformed-ENSO3.4 coefficient of regression. The ENSO3.4 index is computed in the usual way, as the 3-month rolling average of the mean sea surface temperature of the region 120° W-170° W, 5S°-5N°.

3.1.3 Computing the Hilbert transform of ENSO3.4

The Hilbert transform is a method originating in the field of signal processing that computes a signal whose components are all phase shifted by ± 90° relative to its input. The Hilbert

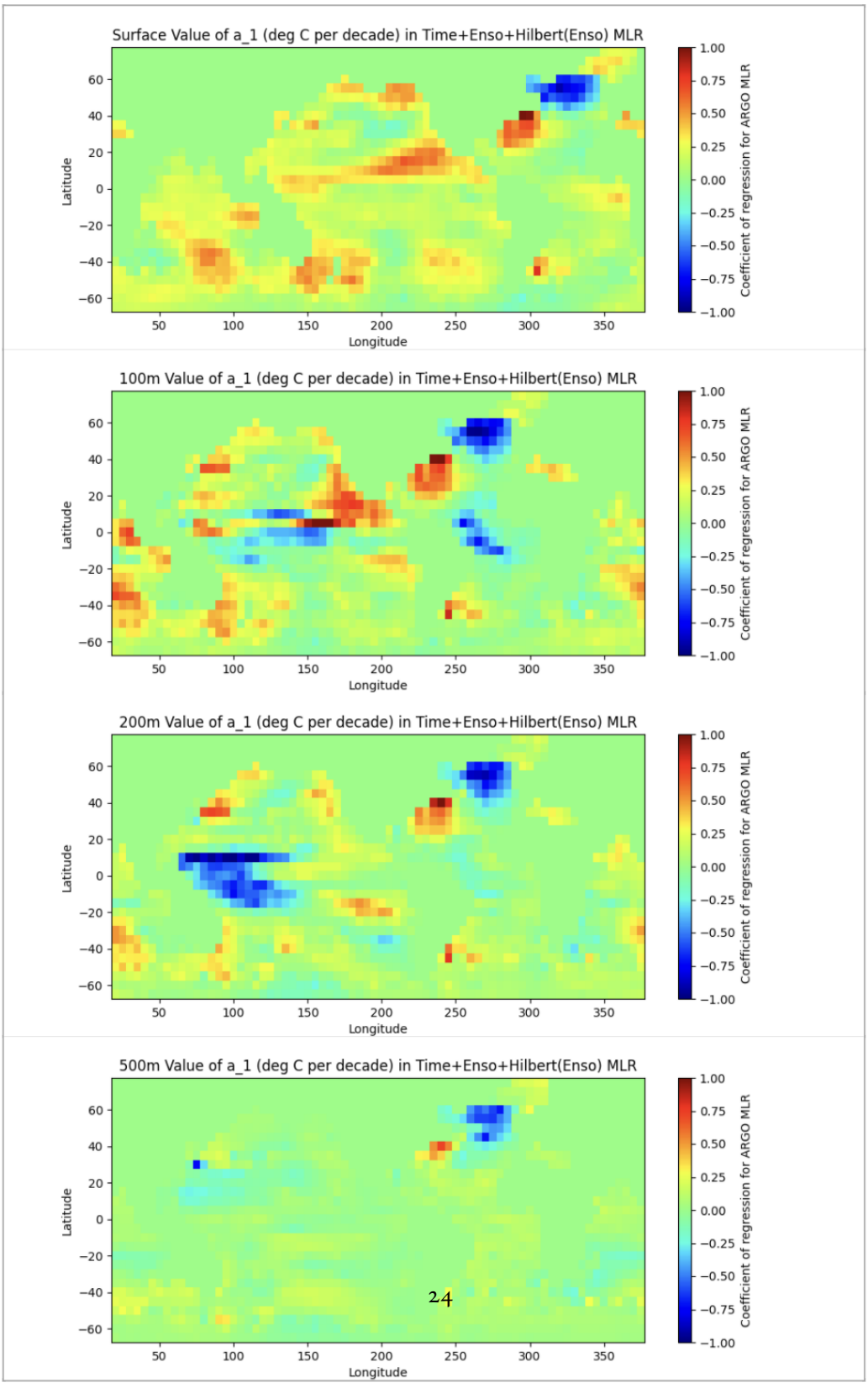

Figure 3.4: Signal strength computed at 0m, 100m, 200m, 500m from multiple-linear against time trends, ENSO3.4 index coefficient, and the hilbert transform of the ENSO3.4 index.

transform of a time-dependent signal $u(t)$ is defined as

$$\mathcal{H}(u(t)) = \frac{1}{\pi} \text{p.v.} \int_{-\infty}^{\infty} \frac{u(\tau)}{t-\tau} d\tau \tag{3.2}$$

where p.v. indicates the Cauchy principal value function, an unimportant mathematical formalism that ensures that the integral converges. $\mathcal{H}$ is equivalent to convolution with $\frac{1}{\pi t}$. Applying the Hilbert transform to the ENSO3.4 index a useful way to allow for linear regression against two orthogonal ENSO-driven modes; figure 3.2 indicates that orthogonal modes whose pattern resembles that of ENSO represent the second- and third- strongest modes of variability in the near-surface ocean, the first- and second- strongest modes of natural variability at 200m, and apparently the first- and third- strongest modes of natural variability at 500m.

The Hilbert transform is computed on the ENSO 3.4 index for years 2001-2021, and then the first three and last three years are disregarded during the regression. This is because the discrete version of the transform degenerates near its bounds. Figure 3.5 shows that the Hilbert transform of the ENSO3.4 index is orthogonal to the original, and shows the effect of the correction done near the bounds.

Figure 3.4 shows the coefficient of regressions for ENSO and its Hilbert transform a_2 and a_3 respectively, displayed next to the primary ENSO-driven modes of variability at depth levels 0m, 100m, and 200m. There is a clear correlation between the absolute values of the

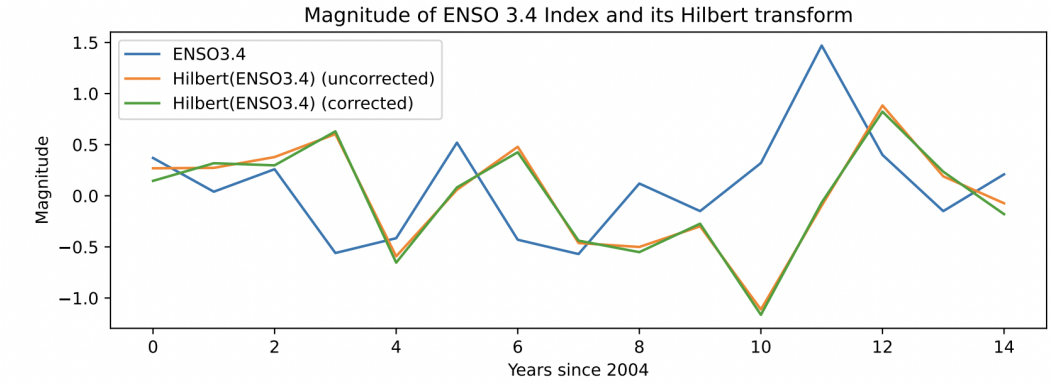

Figure 3.5: The ENSO3.4 index, computed from monthly Argo SST 2004-2018 and then annualized, contrasted with its Hilbert transform, and the corrected Hilbert transform to account for degeneracy of the discrete Hilbert transform near its bounds.

coefficients of regression and of the singular values, indicating that our regression can provide a systematic way to account for the modes of variability. The correlation decreases with depth; as the influence of ENSO wanes at high pressure, the primary singular values of ocean heat content change become increasingly independent from ENSO.

3.2 Computation of optimal fingerprint

An optimal two-dimensional fingerprint is computed at 34 depth levels in the upper 2000m per the fingerprinting method discussed in chapter 2.

A multiple linear regression is computed as in (3.1) on 200 years of ACCESS data, which comprises of 4 chunks of monthly climatology 1850-1900 concatenated to form a synthetic timeseries of 200 years in length. We model each the temperature of each point of model data

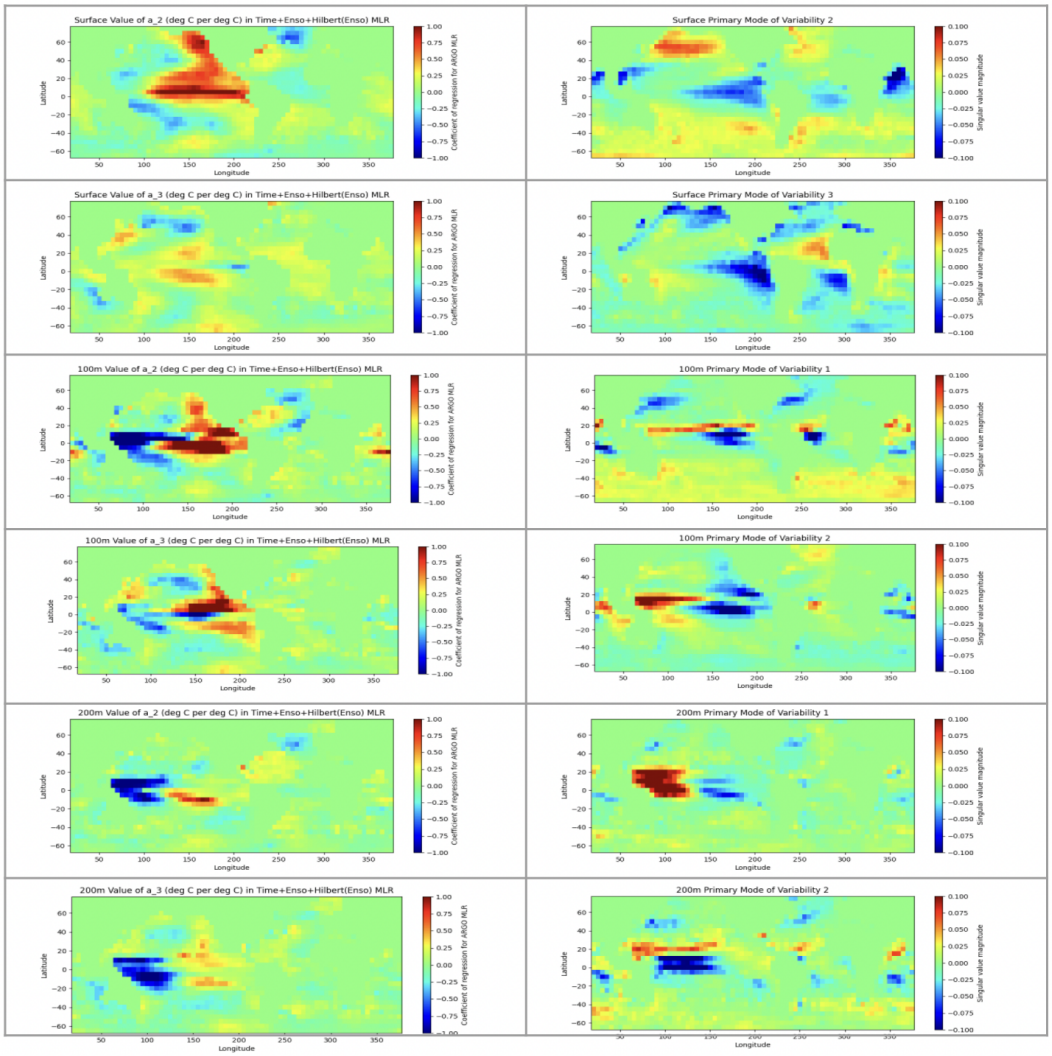

Figure 3.6: The spatial values of coefficients a_2 and a_3 (left) corresponding to the strength of the linear trend explained by ENSO and the Hilbert transform of ENSO, contrasted with the primary modes of oceanic thermal variability, as determined by SVD, at depths 0m, 100m and 200m (right). The first mode of thermal variability at the surface, which is consistent with the seasonal cycle, is omitted.

2.5m	10m	20m	30m	40m	50m	60m	70m
80m	90m	100m	110m	120m	130m	140m	150m
160m	170m	180m	190m	200m	215m	240m	280m
343m	427m	536m	665m	810m	970m	1130m	1290m
1450m	1620m	1800m	2000m				

Figure 3.7: Depths at which optimal fingerprint is computed. 2000m is the deepest depth for which data from both Argo and ACCESS are available.

$\theta'(t)$ as

$$\theta'(t) = (a'_1 \times t) + (a'_2 \times E') + (a'_3 \times H') + e'(t) \tag{3.3}$$

where a'_1, a'_2, and a'_3 are the coefficients of regression corresponding to t, E', the model ENSO3.4 index, and H', the Hilbert transform of the model index, respectively. The model ENSO3.4 index is calculated identically to the ENSO3.4 index on Argo data. Independent calculation of this index for model data is important; although ACCESS is the most skillful of the models in CMIP in accurately depicting the spatial pattern of interannual variability, it does not correlate perfectly with observational data; hence the location of ENSO in the ocean of the ACCESS model is not identical to that of data obtained from Argo floats (Coburn & Pryor,

2021).

The fingerprint f_p at pressure level p is given by

$$f_p = C_p^{-1} a_{1,p} \tag{3.4}$$

where C_p^{-1} is the covariance matrix of residuals $e'_p(t)$ from the regression done in 3.3, and $a_{1,p}$ is from 3.1.

3.2.1 Approximate matrix inverses

Although optimal fingerprinting calls for C_p^{-1} to be computed, the inverse of C_p is not always defined. We use a generalization of the definition of a matrix inverse, known as a Moore-Penrose pseudoinverse to accommodate this situation. Let $A \in \mathbb{R}^{n \times k}$ have SVD USV^T, where $U \in \mathbb{R}^{n \times r}$ and $V \in \mathbb{R}^{d \times r}$, and where $S \in \mathbb{R}^{r \times r}$ is a diagonal matrix whose diagonal contains the first r singular values of. Then, the Moore-Penrose pseudoinverse of A, denoted $A^\dagger$, is given by

$$A^\dagger = VS^{-1}U^T \tag{3.5}$$

This inverse is motivated by the fact that

$$A^\dagger = VS^{-1}U^T USV = VV^T \tag{3.6}$$

and hence

$$AA^{\dagger}A = AI = IA. \tag{3.7}$$

We invert the C_p matrix inverse with $r = 1$. This coefficient was chosen beacuse SVDs of C_p showed a significant amount of variability could be explained by the first mode, and subsequent modes were poorly determined (see Appendix). To account for the undetermined nature of this inverse, we also perform a ridge-regression with a ridge coefficient $rr \approx 1.01$.

4

Results and discussion

In this analysis, we compute optimal horizontal map fingerprints for measuring changes in ocean heat content in 34 locations throughout the upper 2000m of the ocean. Computed fingerprints correlate closely with the pattern of ocean heat content uptake at each depth, with some noteworthy differences which correspond to the fingerprinting technique's increased weighting of quiescent areas of the ocean. We find that the multiple-linear regression

approach proposed in this work effectively de-couples fingerprint direction that of ENSO while remaining correlated with signal direction, suggesting a greater sensitivity of the resultant fingerprint to ocean heat content trends. We identify clear warming pattern in the corresponding detection variables; when averaged across all pressure levels, we find that the 95 % confidence interval of detection variable strength derived from ACCESS-ESM-1.5 historical simulations is exceeded in recent years.

4.1 Computed optimal fingerprints

Optimal fingerprints are computed according to the methods laid out in the previous chapter. Figure 4.1 shows the computed optimal fingerprints at 0, 100m, 200m, and 500m. The fingerprints decrease in magnitude with increasing depth, consistent with the weaker pattern of warming experienced at greater depths. However, fingerprint magnitude decreases much more slowly with depth than that of the signal (Figure 3.4), underscoring the usefulness of fingerprinting in three-dimensions: although the signal of climate change is much weaker at these depths, noise is greatly reduced relative to the surface of the ocean, creating favorable conditions for signal detection. The optimal fingerprints are similar to signal direction at each depth level (see Figure 4.3 for exact correlations), with a few notable exceptions. At the surface, the Western Pacific is emphasized more strongly than in the signal, indicating that the relatively low temperature variability outside of ENSO and the seasonal cycles in the re-

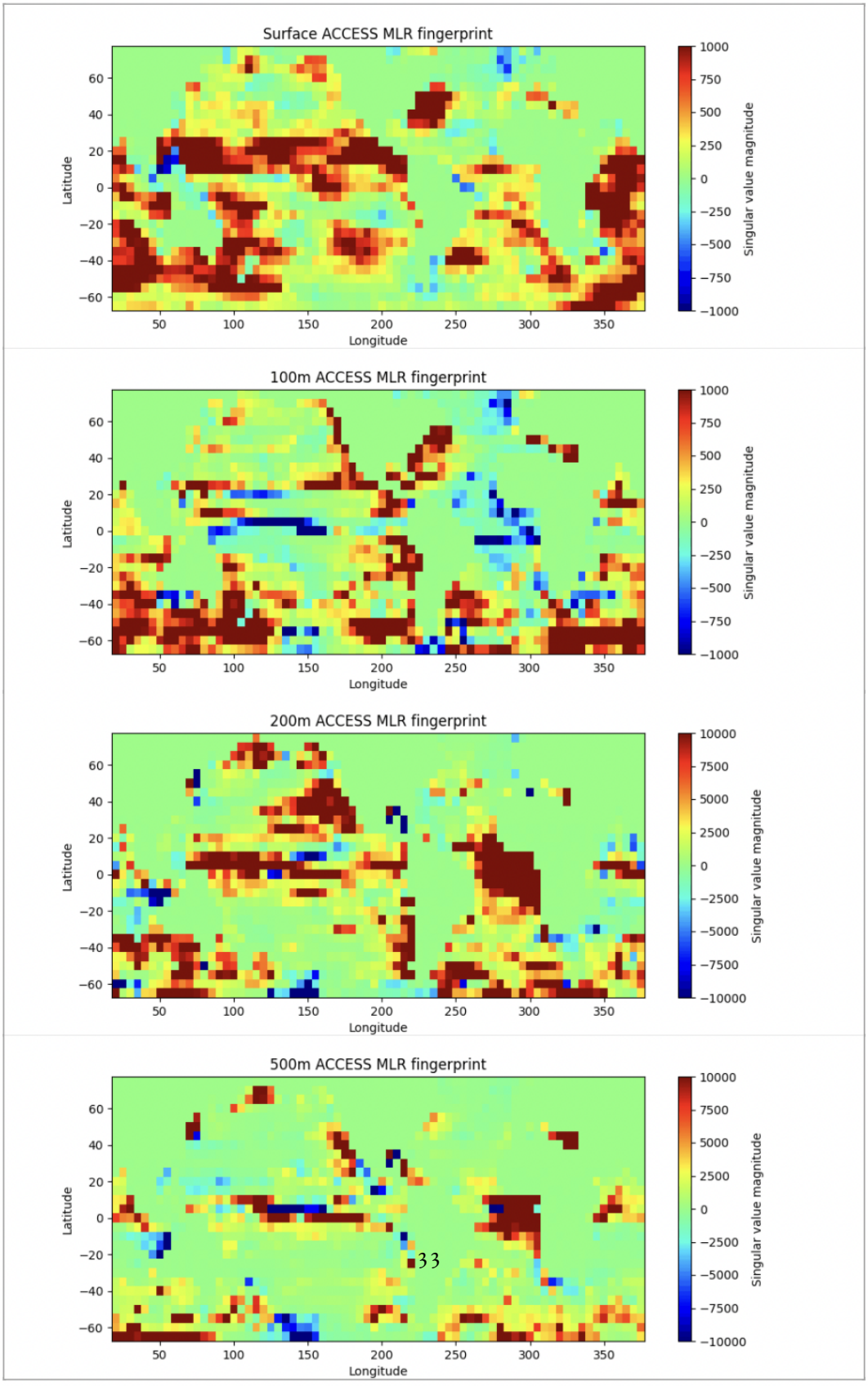

Figure 4.1: Computed fingerprints at 0, 100m, 200m, and 500m. Note the general warming pattern punctuated by areas of cooling.

gion render it more favorable for signal detection. Note also the decreasing prominance of the negatively-weighted portion of the North Atlantic with depth. The signals at 200m and 500m depths (Figure 3.4) feature a strong gradient in linear temperature trend from North to South consistent with the North Atlantic Oscillation (Wanner et al., 2001). The reduced fingerprint weighting here is consistent with the extra noise that accompanies such an oscillation.

4.1.1 Effectiveness of multiple-linear-regressionto account for modes of interannual variability

One of the main novelties of this thesis is the use of a multiple-linear regression to account for modes of interannual variability related to ENSO. Here we show that this technique likely increases the skill the resulting fingerprints; their correlation with the direction of ENSO decreases yet their correlation with the direction of the time signal of ocean heat content increases remains constant.

Figure 4.2 shows two optimal fingerprints on Argo data, computed at the surface with a covariance matric derived from ACCESS data, using the typical signal of ocean heat content change. One is computed using the covariance matrix of the residuals of a multiple-linear regression (top), and another is computed only the residuals of a simple de-trend (second). The fingerprint computed with correction for ENSO is less correlated with the linear coefficient of ENSO strength (third) than the fingerprint computed with only a de-trend. In the fourth

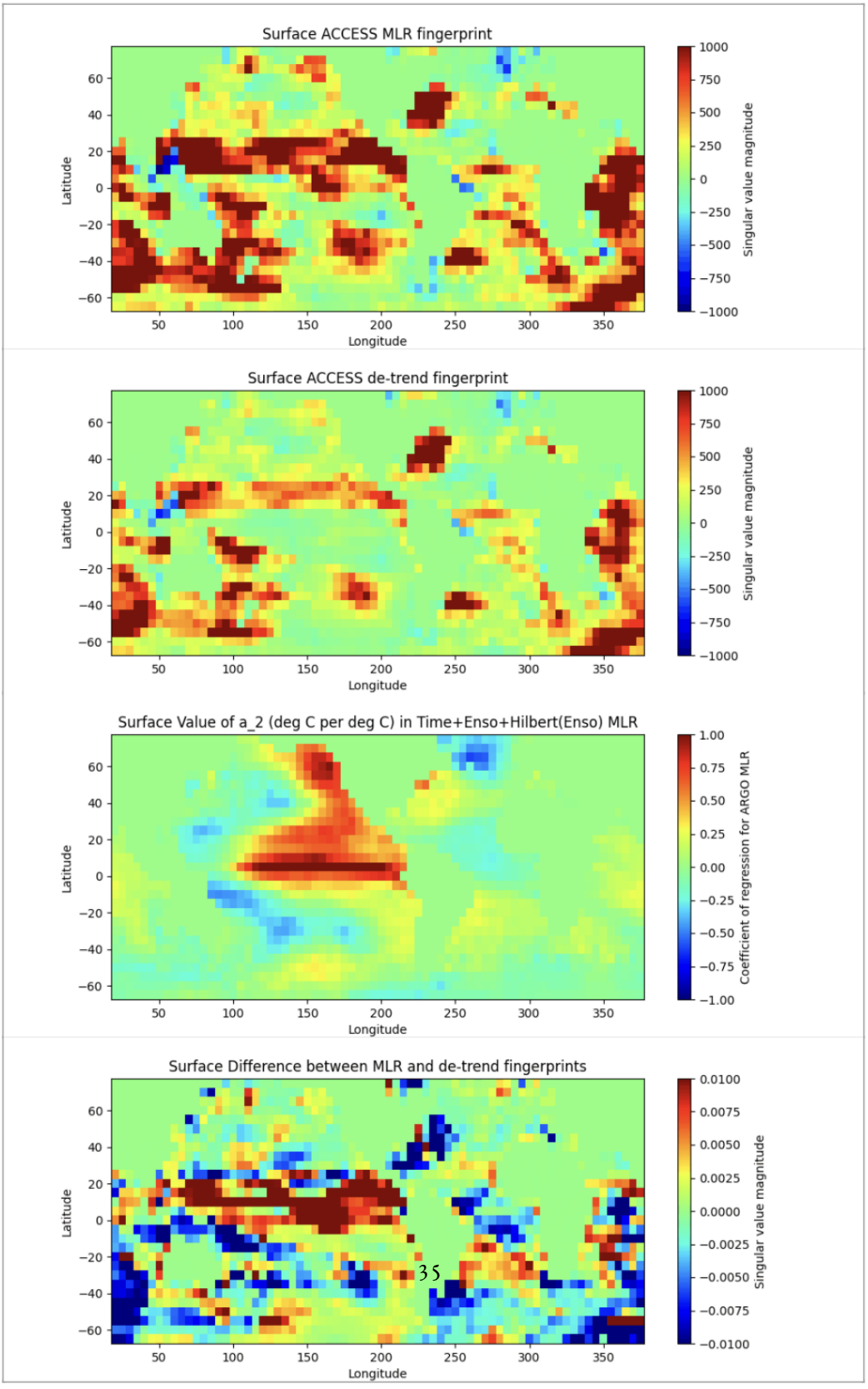

Figure 4.2: Difference between detrended fingerprints and those computed with an MLR.

panel is the difference between the fingerprint computed with the MLR and the fingerprint computed with only a simple de-trend. The two fingerprints differ in areas where the coefficient of ENSO strength is weak, further corroborating the hypothesis that the distortion in the naively-computed fingerprint is due to the covariances caused by ENSO. Both fingerprints display an anticorrelation of the equatorial and Northwest pacific, likely on account of the lower noise content of the region.

Figure 4.3 makes quantitative the correlations between each fingerprint and the directions of the time signal of warming and the strength of the ENSO3.4 index. Both signals are well-correlated with signal direction at all pressure levels down to 1700m, however the fingerprint computed without an MLR to account for ENSO is more highly correlated with the ENSO3.4 at low pressure levels. Note that the correlation of both fingerprints with ENSO approaches zero at higher pressures, showcasing the lesser role ENSO plays in the climatology of the ocean below the near-surface. The decreased correlation of the optimal fingerprint computed with an MLR to account for ENSO with ENSO, yet roughly equal correlation with signal strength indicates that this fingerprint likely has greater correspondance to the optimal detection direction for changes in ocean heat content.

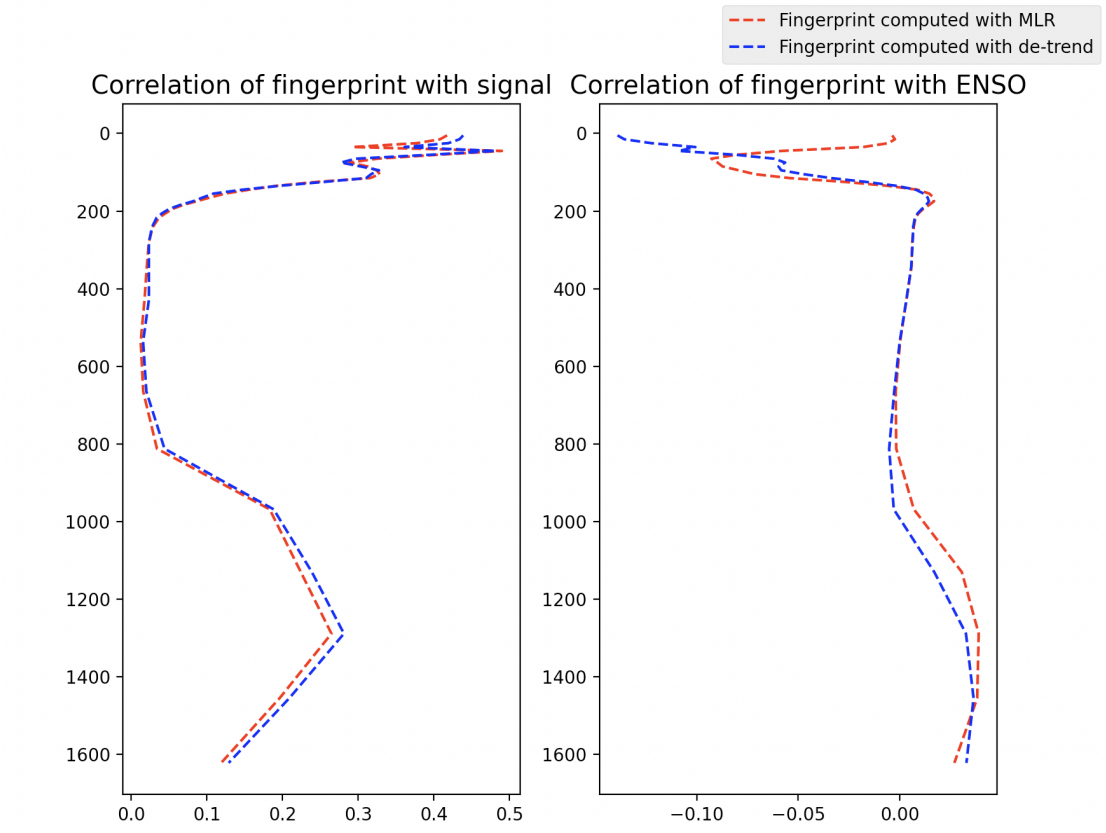

Figure 4.3: Difference between detrend and MLR correlations with signal and ENSO3.4 index. Note the larger negative correlation with ENSO near the surface of the de-trend fingerprint.

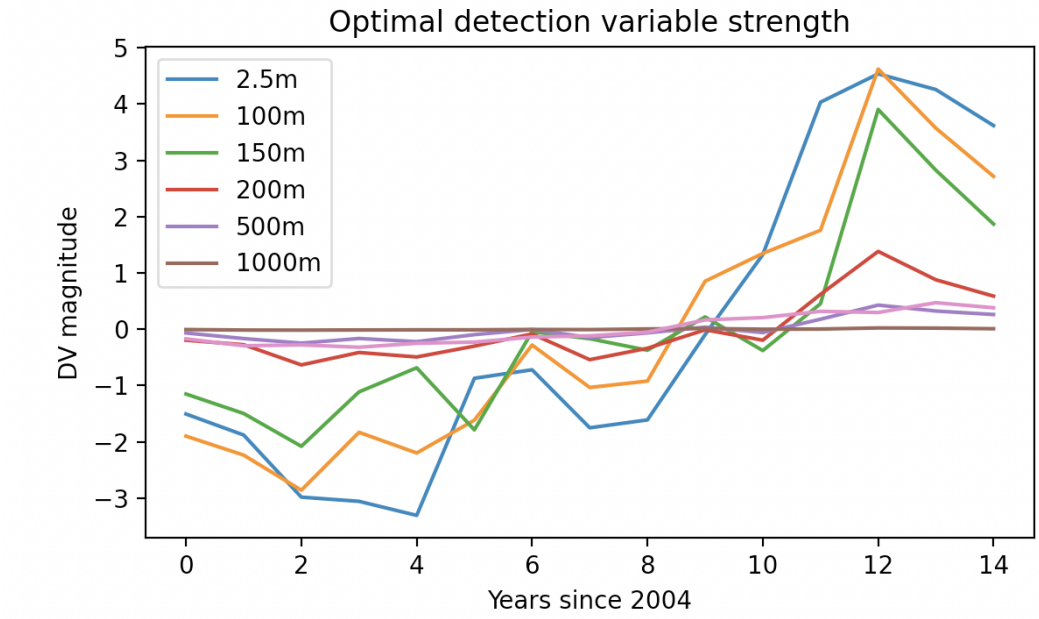

Figure 4.4: Strength of detection variable at various depths. Note how detection variable strength decreases rapidly with depth. All detection variables are normalized to have a mean of 0.

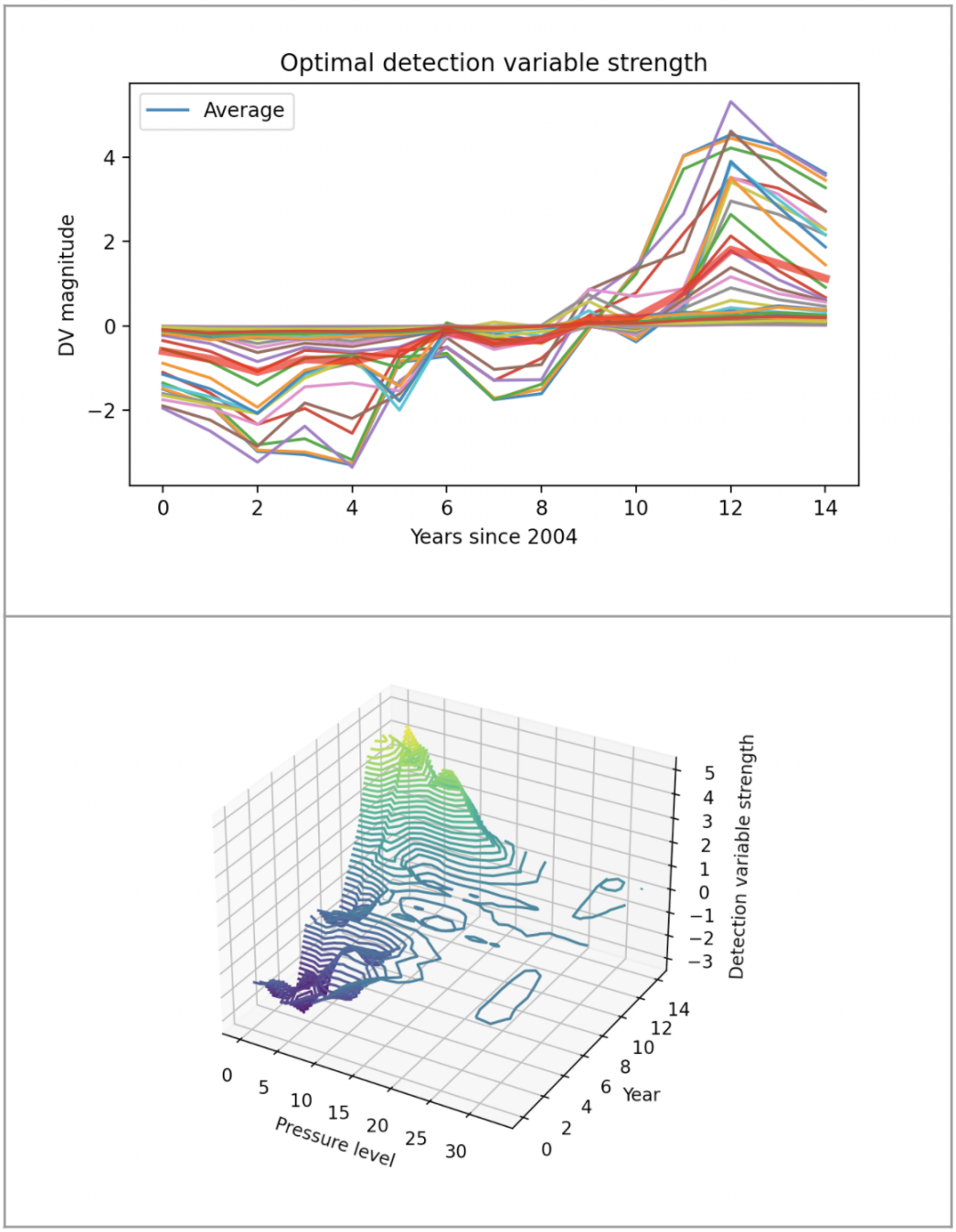

Figure 4.5: Dependence of detection variable on depth. Note how detection variable strength decreases rapidly with depth. All detection variables are normalized to have a mean of 0.

4.2 Detecting a time-dependent uptake of ocean heat

Using the computed optimal fingerprints, optimal detection variables, as described in chapter 2 are calculated to assess the trend in ocean heat content over time. The detection variables exhibit a general warming pattern over the 15-year period 2004-2018 for which our analysis is conducted. Figure 4.4 shows the relative strength of the optimal detection variable at various reference depths. The magnitude of the increase of the optimal detection variable drops off dramatically past 200m, consistent with the physical processes that govern ocean heat uptake. However, the rate of change of magnitude of the detection variable is generally positive, confirming that ocean heat content has increased appreciably in the last two decades. Figure 4.6 displays in the top panel all 34 fingerprints computed at depth levels 0-34, confirming a general warming trend at all levels of the ocean. The bottom panel plots all 34 of these curves onto a 3D contour ploy, displaying the much higher rate of change of the optimal detection variable at lower pressures.

4.3 Significance

Significance of the trend in the optimal detection variable is assessed relative to the behavior of the unforced climate. The computed set of 34 optimal fingerprints was applied to 100 years of ACCESS-MLR-ES1.5 data with minimal forcing, and a 95% confidence interval of detection variable strength due to natural variability was established. Figure 4.6 depicts de-

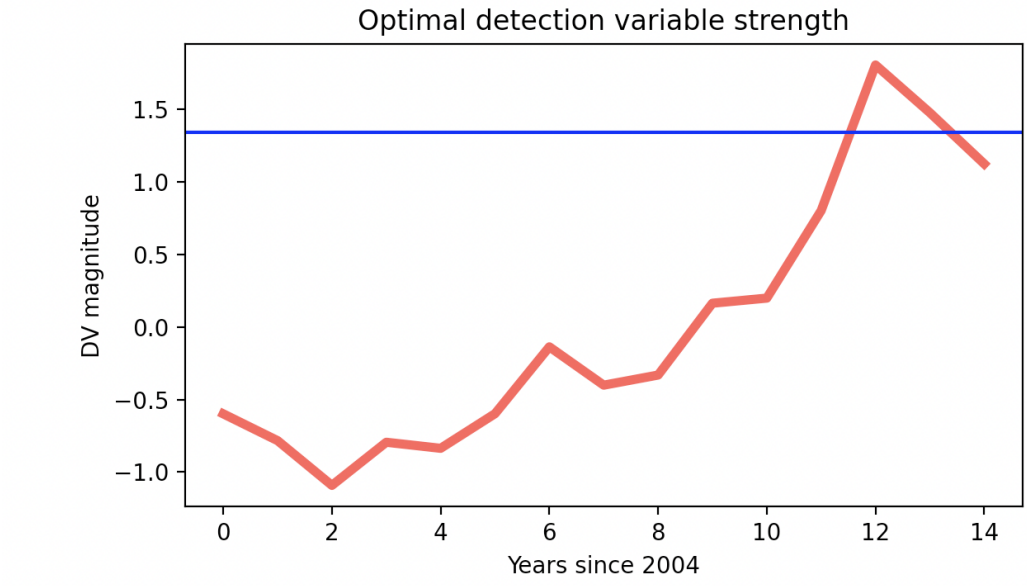

Figure 4.6: Average detection variable strength on 15 years of Argo data across 34 pressure levels versus the 95 % threshold of natural variability for the same quantity, as determined by 100 years of simulation from the ACCESS-ESM-1.5 model.

tection variable strength relative to this confidence interval, and shows two years– 2016 and 2017– were characterized by values of the average optimal detection variable which exceeded the threshold. The conclusion can hence be drawn that during this period, ocean heat content has increased in a significant way according to the signal direction described in Figure 3.4.

5

Conclusion and future directions

In this analysis, an optimal fingerprint is computed on three-dimensional ocean heat data from Argo from 2004-2018 against natural variability computed with the ACCESS-ESM-1.5 climate model. A signal of change in ocean heat content is developed via regressing against time. A novel method for accounting for the modes of natural variability corresponding to ENSO is proposed and applied, and shown to have a positive impact on the skill of the

resultant fingerprint. Optimal detection variables are derived from the computed optimal fingerprints, and their application against Argo data reveals a statistically significant extreme in ocean heat content in the direction of the time signal of change in ocean heat content, indicating an increase in ocean heat content across the upper 2000m of the global ocean. Although further research is required to confirm the results presented here, this finding carries significant consequences to future adaptation to climate change-induced rising sea levels.

5.1 Future directions

Future work will focus on extending the results presented here, and increasing certainty in their significance. In this work, fingerprints are computed at only two dimensions at a time; this is due to the limitations in the compute available for this project. However, the methods presented here can be extended in a straightforward way to three-dimensional fingerprints of ocean heat content. Further correction for modes of interannual variability via MLR is also desirable. A promising candidate for this direction is correction for the North Atlantic Oscillation, whose influence on our determined signal of ocean heat content change appears to be felt heavily in the 200-500m depth range. Finally, this work does not attempt to provide attribution to the observed changes in ocean heat content to any particular cause. While it is reasonable to hypothesize that anthropogenic climate change is the origin of these changes, we do not establish this with any certainty here. Hence, it would be sensible to proceed with

attemp to make an attribution of these changes to climate change, in the same spirit as other optimal fingerprinting studies such as Hegerl et al. (1996) or Barnett et al. (2004)

References

Barnett, T. P. et al. (2004). Penetration of human-induced warming into the world's oceans. *Science*.

Church, J. A. et al. (2011). Revisiting the earth's sea-level and energy budgets from 1961 to 2008. *Geophysical Research Letters*, 38(18601).

Church, J. A. et al. (2013). *Climate Change 2013: The Physical Science Basis. Contribution of Working Group I to the Fifth Assessment Report of the Intergovernmental Panel on Climate Change*. Cambridge University Press.

Coburn, J. & Pryor, S. (2021). Differential credibility of climate modes in cmip6. *Journal of Climate*.

de Boyer Montégut, C. et al. (2004). Mixed layer depth over the global ocean: An examination of profile data and a profile-based climatology. *Journal of Geophysical Research*, 109(12003).

Gebbie, J. & Huybers, P. (2019). The little ice age and 20th century deep pacific cooling. *Science*, 363(6422).

Glecker, P. et al. (2012). Human-induced global ocean warming on multidecadal timescales. *Nature climate change*.

Glecker, P. et al. (2015). New perspectives on observed and simulated antarctic sea ice extent trends using optimal fingerprinting techniques. *Journal of Climate*.

Hasselmann, K. (1979). On the signal-to-noise problem in atmospheric response studies. *Meteorology of Tropical Oceans*.

Hasselmann, K. (1993). Optimal fingerprints for the detection of time-dependent climate change. *Journal of Climate*.

Hegerl, G. et al. (1996). Detecting greenhouse-gas-induced climate change with an optimal fingerprint method. *Journal of Climate*.

Jorda, G. et al. (2020). Ocean warming compresses the three-dimensional habitat of marine life. *Nature Ecology and Evolution*, 4.

Kulp, S. A. & Strauss, B. H. (2019). New elevation data triple estimates of global vulnerability to sea-level rise and coastal flooding. *Nature Communications*, 10(4844).

Levitus, S. et al. (2012). World ocean heat content and thermosteric sea level change (0–2000 m), 1955–2010. *Geophysical Research Letters*, 39.

Lyu, K. et al. (2021). Projected ocean warming constrained by the ocean observational record. *Nature Climate Change*, 11.

Min, S.-K. et al. (2011). Human contribution to more-intense precipitation extremes. *Nature*.

Penduff, T. (2018). Chaotic variability of ocean heat content. *Oceanography*, 31.

Resplandy, L. et al. (2019). Quantification of ocean heat uptake from changes in atmospheric o_2 and co_2 composition. *Scientific Reports*, 9(20244).

Smith, M. et al. (2018). Episodic reversal of autumn ice advance caused by release of ocean heat in the beaufort sea. *Journal of Geophysical Research Oceans*, 123.

Wanner, H. et al. (2001). North atlantic oscillation – concepts and studies. *Surveys in Geophysics*.

Wunsch, C. (2015). *Modern observational physical oceanography: understanding the global ocean*. Princeton University Press.

Wunsch, C. (2020). Multi-year ocean thermal variability. *Dynamic Meteorology and Oceanography*, 72.

Ziehn, T. et al. (2019). The australian earth system model: Access-esm1.5. *Journal of Southern Hemisphere Earth Systems Science*.

This thesis was typeset using LaTeX, originally developed by Leslie Lamport and based on Donald Knuth's TeX. The body text is set in 11 point Egenolff-Berner Garamond, a revival of Claude Garamont's humanist typeface. A template that can be used to format a PhD dissertation with this look & feel has been released under the permissive AGPL license, and can be found online at github.com/suchow/Dissertate or from its lead author, Jordan Suchow, at suchow@post.harvard.edu.